Structural Evolution of a Cyclooctatetraene Adlayer on Cu(111) During Isothermal Desorption

JA Lau,[†,¶] I Calvo-Almazán,[†,§] PSM Townsend,[†] DJ Ward,[†] AP Jardine,[†] W Allison,[†] J Ellis,[†] BJ Hinch,[‡] and N Avidor*[,†]

†*Cavendish Laboratory, University of Cambridge, JJ Thomson Avenue, Cambridge CB3 0HE, United Kingdom*

‡*Department of Chemistry and Chemical Biology, Rutgers University, Piscataway, New Jersey 08854, USA*

¶*Present address: University of Goettingen, Institute of Physical Chemistry, Tammannstr. 6, 37077 Goettingen, Germany*

§*Present address: Material Science Division, Argonne National Laboratory, Argonne, 60439, Illinois, United States*

E-mail: na364@cam.ac.uk

Abstract

The use of helium diffraction patterns to study desorption processes is explored as a novel extension to traditional methods based on helium specular reflection. The sample, cyclooctatetraene adsorbed on Cu(111), provides a rich but complex structure. The modulation of cyclooctatetraene by Cu(111) is manifested as a convolution in the diffraction pattern, displaying an averaged super-cell symmetry of $(7\sqrt{3} \times 7\sqrt{3})R30°$. The adlayer expands during isothermal desorption, and the change in lattice constant provides a direct measure of the coverage as a function of time. We find a desorption energy of 0.96 ± 0.01 eV at saturation of the first layer, and an upper limit of 1.62 ± 0.07 eV for isolated molecules. These values, and details of the assigned structure, indicate chemisorbed molecules with a planar conformation.

Introduction

The growing importance of organic electronics[1] is driving an increasing effort to understand and control organic-metal interfaces.[2–4] Molecular interactions and the dynamical behavior of molecules at technologically relevant temperatures, and at multilayer coverages, are some of the open questions which are difficult to address with conventional experiments.[5,6] When a gentle probe or supreme surface sensitivity is required, helium diffraction is particularly useful. Helium beam energies are typically below 10meV, and atoms scatter from the outer-most surface electrons. Hence the neutral atoms do not damage organic layers, and are highly sensitive to even low densities of adsorbates.

Organic thin-films often present coverage and temperature dependent structures. A powerful means to explore the interplay of inter-adsorbate and adsorbate-substrate interactions,[7,8] which dominate the structures, is by studying the evolution of structure with temperature, and during desorption. The properties of organic-metal interfaces are known to be affected by the adsorption state and charge-transfer.[9–11] It is therefore of interest to study cyclooctatetraene (C_8H_8, COT), which is known to undergo conformational changes with

charge transfer. In the gas phase, neutral COT has a tub-like conformation and a four-fold or an aromatic eight-fold symmetry, for the singly or doubly charged ion, respectively.[12–14]

There is also experimental evidence for varying conformations of adsorbed COT molecules.[12,15–17] The tub-geometry of COT was observed in multilayers and 3D solid phases.[12,15,16] In contrast, the adsorption properties in the first layer are more diverse. Harutyunyan et. al.[17] performed low temperature scanning tunneling microscopy (STM) studies of COT on Au(111), Ag(100) and Cu(100). The binding strength increased from Au(111), with physisorbed tub-shaped COT, to Ag(100) and Cu(100) where chemisorbed planar species were found. While planar COT can be formed upon charge transfer in the gas phase, the DFT calculations suggested that the binding involves strong hybridization with metal states, with minimal charge transfer.[17] Alternatively, a study of COT on Ag(110) demonstrated the significance of charge states in the monolayer structure, where electron energy loss spectroscopy (EELS) shows a planar species for the clean surface while the oxygen-precovered surfaces show vibrations typical of the tub-shaped molecule.[15] Covalent binding is found on Si(001).[18] On Ru(001),[12] Pt(111)[19] and Pd(111),[20] COT was found to have a variety of adsorption states and a tendency to decompose upon desorption. On Cu(111) however, COT stays intact upon desorption.[21] More generally, COT is of technological interest, and potential applications in organic LEDs have already been demonstrated using substituted COT derivatives.[22,23]

Here we report on the diffraction of helium from a COT adlayer adsorbed on Cu(111). The structure is inferred using the convolution theorem in the framework of the eikonal approximation for helium scattering. A novel extension to helium specular-reflection based, time-resolved isothermal studies[24–27] is demonstrated. By measuring the evolution of diffraction peaks at elevated temperatures, we obtain direct information on the change in coverage during isothermal desorption. We extract the desorption energy of COT at monolayer coverage and estimate an upper limit for the desorption energy of isolated COT molecules. The possibility to directly measure domain-dependent desorption energies is discussed as well.

Experimental Methods

The diffraction experiment was performed at the Cambridge Helium scattering facility using a ^{3}He Spin-Echo spectrometer,[28,29] which is designed primarily for measurements of surface dynamics. The probe was a supersonic beam of helium-3, with a mean beam energy of 8.25 meV. The full width at half maximum (FWHM) of 0.86 meV determines the resolution in reciprocal space, which varies from 0.07 to 0.14Å^{-1} increasing with momentum transfer in the experimental range. The surface temperature was regulated with liquid nitrogen cooling and radiative heating. The Cu(111) crystal was cleaned using cycles of argon ion sputtering for 20 minutes at 300 K (0.8 kV, 6-9 μA), followed by flash annealing to 850 K. The quality of the crystal surface was verified by measuring the specular helium reflectivity, which is sensitive to metallic surface defect densities of below 1%.[30] Helium reflectivity after cleaning exceeded 40%, indicating an extremely clean and flat surface. Cyclooctatetraene (Sigma Aldrich, 98%) layers were grown by backfilling the chamber (typically at 1-2 $\times 10^{-8}$ mbar) while recording the helium signal to monitor the growth. Prior to dosing, the COT was purified to remove dissolved gas contamination by repeated freeze-pump-thaw cycles using liquid nitrogen. 2D diffraction patterns were measured by rotating the surface normal within the scattering plane (angular scans) for different azimuthal orientations of the crystal.

Results and Discussion

We first report on a well defined diffraction pattern at 205 K, and its assigned structure. Later follows the description of isothermal desorption measurements, which imply a coverage-dependent desorption energy.

Figure 1(a) presents a diffraction pattern at 205 K after dosing COT to saturation at 230K, which is above the multilayer desorption point (around 210 K).[21] The statistically significant diffraction peaks have been labeled 1-13. A table with peak positions and intensities, and a representation of a full 2D diffraction pattern (composed by replicating the actual measured pattern), are provided in the Supporting Information (SI). The most intense peaks in figure 1(a) - 4, 8 and 11 - exhibit hexagonal symmetry, which is rotated by 30° relative to the diffraction pattern of the Cu(111) surface. The symmetry is attributed to an azimuthally aligned hexagonal close-packing of the COT molecules, with a lattice constant of 7.70-7.75 Å, and can be written as $(3 \times 3)R30°$ as shown in figure 2. Assuming the surface is homogeneously covered, the structure implies a number density of 0.11 with respect to the substrate surface atoms. Using calculated bond lengths[14] and a van der Waals radius of 1.01Å for hydrogen along the C-H bonds,[31] the van der Waals radius of the planar COT dianion is estimated to be 4.0Å, giving a diameter of 8Å. The similarity with the experimental lattice constant, combined with the expectation of highly symmetric molecules to prefer a close-packed structure, suggests that COT adopts a planar, benzene-like conformation at monolayer coverages.

The hexagonal COT lattice seems to coincide with the Cu(111) lattice to give a $(7\sqrt{3} \times 7\sqrt{3})R30°$ super-cell. While the diffraction pattern is consistent with the super-cell symmetry, possible peaks are missing, that cannot be attributed to systematic extinctions. Close inspection of the diffraction pattern, including the apparent absence of peaks, shows that it can be qualitatively explained by a convolution. As we derive in the supporting information, if the corrugation functions for the adsorbate and substrate-induced modulation have additive components, then under the eikonal approximation, the diffraction amplitude F is a convolution of two diffraction amplitudes - from an ordered adsorbed overlayer, F_a, and from a substrate-induced modulation of the overlayer, F_s, and can be written as:

$$F(\mathbf{\Delta K}) = \frac{S_a S_s}{S}(F_a * F_s)(\mathbf{\Delta K}). \qquad (1)$$

Here $\mathbf{\Delta K}$ is the surface-parallel momentum transfer of the helium atom, and S, S_a and S_s are the surface areas of the super-cell, adsorbate and substrate unit-cells, respectively. Importantly, the derivation does not assume commensuration of the adlayer. Peaks predicted by the convolution in Eq.1 are shown in Figure 1(b) where they are superimposed on the data. Black squares show the expected positions of diffraction peaks related to the COT lattice. Empty white circles show the peaks arising from convolution of the adlayer G-vectors with the six lowest-order substrate G-vectors, while crosses indicate the expected peak positions arising from convolution with higher-order G-vectors of the substrate. The absence of peaks 15-17 in the experimental diffraction pattern can be explained in terms of low amplitude, F_a, at large values of $\Delta\mathbf{K}$, combined with weak higher-order modulation by the substrate, F_s. Peak 14, which is barely detected above the noise level, should not be attenuated by a convolution with substrate-induced higher-order modulation. While the low intensity may be a result of (reciprocal) distance from specular (away from $\Delta\mathbf{K} = 0$), we can not exclude form-factor effects. Two peaks marked as 2 and 5 in figure 1(a) are not explained by the superstructure suggested above, but are attributed to the most intense peaks of a non-rotated structure (equivalent to peaks 8 and 11, but lower in two orders of magnitude) with a slightly smaller lattice constant of 7.64 Å.

Close inspection of the azimuthal dependence of the three most intense peaks (4, 8 and 11 in figure 1) shows maxima which are separated by $\approx 0.6°$ as seen in figure 3. These features suggest that the structure of the COT adlayer is more complicated than described so far. The satellite peaks are normally an indication of still larger order superstructures with ordered arrays of domain walls.[32,33] However, the fact that 4 or more peaks of one narrow azimuthal scan ($-1° < \Delta\alpha < 1°$) can display remarkably similar intensities, suggests that the diffraction is

resulted from coexisting domains with a narrow distribution of azimuthal orientations (around $R30^\circ$). A more detailed analysis of the higher order commensuration and/or domain distribution would require a finer azimuthal scan and an enhanced momentum transfer resolution, which was not attained at the time of the experiment.

To summarize, the dominant structure in the COT adlayer is an approximate $(3 \times 3)R30^\circ$ structure, with evidence that a small fraction of the adlayer is influenced by small surface defect densities, forming a rotated structure with comparable lattice constant.

The alignment of the COT adlayer with the substrate on the one hand and the formation of a closed-packed structure on the other hand, suggest that repulsive interactions between the COT molecules and adsorbate-substrate interactions are of similar importance at 205 K. An insight into the interplay between the two types of interactions can be obtained from desorption measurements. Earlier mass analyzed TPD measurements of COT desorbing from Cu(111) show three desorption peaks (labeled α, γ, β).[21] Peaks α and γ are of the multilayer and monolayer, respectively. We assign the β peak, which rises simultaneously with the multilayer peak, to the second adsorbed layer. The simple Redhead approximation[34] can be applied to the first order desorption shown by the γ peak. With the peak temperature of 475 K and assuming a prefactor of 10^{13} sec^{-1}, the average desorption energy is found to be 1.3 eV.

The rather large energy (desorption temperature), together with the planar conformation of the molecule as discussed earlier, allow us to conclude the molecule is chemisorbed in a planar configuration. Determining the nature of bonding, e.g. hybridization with metal surface states as suggested in Ref.[17] or charge transfer to COT, which produces a planar molecule in the gas phase, requires supplementary experiments and further calculations.

We now turn to a novel (though natural) extension of helium specular-reflection based, time-resolved desorption measurements - where diffraction peaks are monitored instead of the specular peak. At a temperature of 300 K, the role of repulsive interactions can be studied by the expansion of the structure over time, which we attribute to continuous desorption of COT for large coverages. The isothermal desorption experiment was performed as follows: COT is dosed to saturation at 300 K. After the exposure is stopped, peak 8 is monitored repetitively using four 2D diffraction scans, so that the change in peak shape with time can be determined. Figure 4(a-b) presents the equivalent of angular and azimuthal scans, respectively, through the maximum of peak 8 (extracted from each 2D scan). Initially, the azimuthal shape (figure 4(b)), and the lattice constant as extracted from the peak position in the angular scan (figure 4(a)), are comparable to the structure measured at 205 K (figures 1 and 3). However, with time, the peak position in figure 4(a) shifts closer to specular, suggesting the structure expands. Furthermore, with expansion, the azimuthal peak broadens, implying that the distribution of domains (as seen in the fine sub-peaks) becomes more even, resulting-in an apparent azimuthal partial-ring feature. The signs for monotonically growing disorder suggest that the COT does not form islands. Furthermore, we did not see any sign for islanding during deposition of the COT while monitoring the helium specular intensity. The shift of the peak in ΔK, as shown in figure 4(a), provides an estimate of the average lattice constant of the adlayer as a function of time. From the lattice constant, the coverage as function of time can be calculated. Figure 4(c) presents the change in coverage as a function of time, extracted from the angular scans in the azimuthal range of 27.5-32.5 degrees, which form the four 2D diffraction scans around peak 8. The Polanyi-Wigner equation[35] can be used to extract the coverage dependence of the desorption energy (see SI for details). Since we recorded the change over a small coverage range, we assume a linear dependence of the desorption energy with coverage. Further assumptions are a constant prefactor of 10^{13} sec^{-1} and first-order desorption. In the coverage range of the measurement, the desorption energy changes by less than 0.06 eV with a mean energy of 1.06 eV. Linear extrapolation of the energy gives the desorption

energy as 0.96 ± 0.01 eV at monolayer coverage (as measured at 205 K, equivalent to a number density of 0.11 with respect to the substrate) with 1.62 ± 0.07 eV for isolated molecules in the zero coverage limit. While linear extrapolation to the monolayer coverage is presumably a good approximation, the linear dependence need not hold down to zero coverage and therefore can only suggest an upper limit to the desorption energy of isolated COT molecules. Since the value extracted from the Redhead analysis corresponds to an averaged desorption energy, we expect that the true value for isolated COT molecules lies between 1.3 and 1.6 eV.

It is worth noting that each 2D scan of peak 8 captures the change in lattice constant of all the different domains (as manifested in the sub-peaks), as well as the change in the domain distribution (the change in the sub-peak intensities). Therefore, while our analysis averages over the different domains in a narrow regime of coverage, a more detailed measurement and analysis will allow domain-specific desorption properties to be extracted. Similar to ref.[36] where TPD spectra could be related to structural motifs observed with low-energy electron microscopy (LEEM), the approach of monitoring diffraction peaks during desorption ties structural information to desorption properties. It opens up the possibility of studying desorption kinetics of different coexisting structures, and across phase changes.

Conclusions

Based on diffraction measurements at 205 K we find that COT forms a hexagonal close-packed adlayer at the Cu(111) surface, with $(3 \times 3)R30°$ adlayer symmetry. Peak intensities in the diffraction pattern from a $(7\sqrt{3} \times 7\sqrt{3})R30°$ superstructure are explained with a convolution of the diffraction from the adsorbate, and a modulation induced by the substrate. Fine features in the diffraction peaks suggest that higher order superstructures and even different domains exist, although classifying the domains would require enhanced resolution. From isothermal desorption measurements at 300 K, we find that the desorption energy varies between 0.96 ± 0.01eV at monolayer coverage (number density of 0.11 with respect to the substrate) and an estimate between 1.3 to 1.6 eV for isolated molecules. The dimensions of the molecule, the close packing, and the large desorption energy, suggest that COT adsorbs in a planar conformation and is chemisorbed. The presented work is a novel extension of helium specular-reflection based, isothermal desorption studies. We have demonstrated the power of the technique, and expect that targeted, more detailed experiments could provide a new class of information on various desorption processes.

Acknowledgement For financial support, N. Avidor gratefully acknowledges the Blavatnik Foundation, J.A. Lau acknowledges the ICASEC, P.S.M. Townsend acknowledges the UK EPSRC, I. Calvo-Almazán acknowledges the Ramón Areces Foundation, BJ Hinch acknowledges the NSF (CHE-1565673). The authors thank G. Alexandrowicz for useful discussions.

Supporting Information Available: An archive of raw data files are available at https://doi.org/10.17863/CAM.21663 . A representation of a full diffraction pattern. A table of diffraction peak intensities. A mathematical description of convoluted diffraction patterns within the eikonal scattering approximation. A method for extracting the coverage as a function of time from 2D diffraction scans. This material is available free of charge via the Internet at `http://pubs.acs.org/`.

References

(1) Forrest, S. R. The path to ubiquitous and low-cost organic electronic appliances on plastic. *Nature* **2004**, *428*, 911–918.

(2) Mas-Torrent, M.; Rovira, C. Role of molecular order and solid-state structure in organic field-effect transistors. *Chem. rev.* **2011**, *111*, 4833–4856.

(3) Braun, S.; Salaneck, W. R.; Fahlman, M.

Energy-level alignment at organic/metal and organic/organic interfaces. *Adv. Mater.* **2009**, *21*, 1450–1472.

(4) Virkar, A. A.; Mannsfeld, S.; Bao, Z.; Stingelin, N. Organic semiconductor growth and morphology Considerations for Organic Thin-Film Transistors. *Adv. Mater.* **2010**, *22*, 3857–3875.

(5) Tkatchenko, A.; Romaner, L.; Hofmann, O. T.; Zojer, E.; Ambrosch-Draxl, C.; Scheffler, M. Van der Waals interactions between organic adsorbates and at organic/inorganic interfaces. *MRS bulletin* **2010**, *35*, 435–442.

(6) At elevated temperatures fast dynamics at the surface normally add noise to the image of scanning probe techniques, or even render visualization of an adsorbate impossible. Furthermore, tip-induced motion is likely to bias measurements of weakly bound molecules, e.g. of some organic overlayers.

(7) Witte, G.; Wöll, C. Growth of aromatic molecules on solid substrates for applications in organic electronics. *J. Mater. Res.* **2004**, *19*, 1889–1916.

(8) Forrest, S. R. Ultrathin organic films grown by organic molecular beam deposition and related techniques. *Chem. Rev.* **1997**, *97*, 1793–1896.

(9) Ou, J. Z.; Ge, W.; Carey, B.; Daeneke, T.; Rotbart, A.; Shan, W.; Wang, Y.; Fu, Z.; Chrimes, A. F.; Wlodarski, W.; others, s. Physisorption-based charge transfer in two-dimensional SnS2 for selective and reversible NO2 gas sensing. *ACS nano* **2015**, *9*, 10313–10323.

(10) Stiehler, C.; Calaza, F.; Schneider, W.-D.; Nilius, N.; Freund, H.-J. Molecular adsorption changes the quantum structure of oxide-supported gold nanoparticles: chemisorption versus physisorption. *Phys. Rev. Lett.* **2015**, *115*, 036804.

(11) Roychoudhury, S.; Motta, C.; Sanvito, S. Charge transfer energies of benzene physisorbed on a graphene sheet from constrained density functional theory. *Phys. Rev. B* **2016**, *93*, 045130.

(12) Tegeder, P.; Danckwerts, M.; Hagen, S.; Hotzel, A.; Wolf, M. Structural transition in cyclooctatetraene adsorbed on Ru (001) probed by thermal desorption and two-photon photoemission spectroscopy. *Surf. sci.* **2005**, *585*, 177–190.

(13) Wenthold, P. G.; Hrovat, D. A.; Borden, W. T.; Lineberger, W. C. Transition-state spectroscopy of cyclooctatetraene. *Science* **1996**, *272*, 1456.

(14) Sokolov, A. Y.; Magers, D. B.; Wu, J. I.; Allen, W. D.; Schleyer, P. v. R.; Schaefer III, H. F. Free cyclooctatetraene dianion: planarity, aromaticity, and theoretical challenges. *J. Chem. Theory Comput.* **2013**, *9*, 4436–4443.

(15) Merrill, P. B.; Madix, R. J. Aromatization of 1, 3, 5, 7-cyclooctatetraene and oxydehydrogenation of cis-cyclooctene, 1, 5-cyclooctadiene and 1, 3, 5, 7-cyclooctatetraene on clean and oxygen precovered Ag (110). *Surf. sci.* **1996**, *365*, 701–728.

(16) Claus, K. H.; Krüger, C. Structure of cyclooctatetraene at 129 K. *Acta Crystallogr., Sect. C: Cryst. Struct. Commun.* **1988**, *44*, 1632–1634.

(17) Harutyunyan, H.; Callsen, M.; Allmers, T.; Caciuc, V.; Blügel, S.; Atodiresei, N.; Wegner, D. Hybridisation at the organic–metal interface: a surface-scientific analogue of Hückel's rule? *Chem. Commun.* **2013**, *49*, 5993–5995.

(18) Hovis, J. S.; Hamers, R. J. Structure and bonding of ordered organic monolayers of 1, 3, 5, 7-cyclooctatetraene on the Si (001) surface: surface cycloaddition chemistry of an antiaromatic molecule. *J. Phys. Chem. B* **1998**, *102*, 687–692.

(19) Manner, W. L.; Dubois, L. H.; Girolami, G. S.; Nuzzo, R. G. Carbon- Hydrogen bond activation and cyclodehydrogenation reactions of cyclic C8 hydrocarbons on Pt (111). *J. Phys. Chem. B* **1998**, *102*, 2391–2402.

(20) Lee, A. F.; Baddeley, C. J.; Hardacre, C.; Lambert, R. M. Investigation of an alternative reaction pathway in the cyclization of ethyne to benzene on palladium: cyclooctatetraene on Pd (111). *JACS* **1995**, *117*, 7719–7725.

(21) Kyriakou, G.; Kim, J.; Tikhov, M. S.; Macleod, N.; Lambert, R. M. Acetylene coupling on Cu (111): formation of butadiene, benzene, and cyclooctatetraene. *J. Phys. Chem. B* **2005**, *109*, 10952–10956.

(22) Lu, P.; Hong, H.; Cai, G.; Djurovich, P.; Weber, W. P.; Thompson, M. E. Synthesis of octasubstituted cyclooctatetraenes and their use as electron transporters in organic light emitting diodes. *JACS* **2000**, *122*, 7480–7486.

(23) Adamovich, V. I.; Cordero, S. R.; Djurovich, P. I.; Tamayo, A.; Thompson, M. E.; DAndrade, B. W.; Forrest, S. R. New charge-carrier blocking materials for high efficiency OLEDs. *Org. Electron.* **2003**, *4*, 77–87.

(24) Peterlinz, K.; Curtiss, T.; Sibener, S. Coverage dependent desorption kinetics of CO from Rh (111) using time-resolved specular helium scattering. *J. Chem. Phys.* **1991**, *95*, 6972–6985.

(25) Croci, M.; Félix, C.; Vandoni, G.; Harbich, W.; Monot, R. Chemisorption and macroscopic diffusion of NO on Pt (111). *Surf. sci.* **1994**, *307*, 460–464.

(26) Schaich, T.; Braun, J.; Toennies, J.; Buck, M.; Wöll, C. Structural changes accompanying the hydrogen desorption from the diamond C (111): H (1× 1)-surface revisited by helium atom scattering. *Surf. sci.* **1997**, *385*, L958–L964.

(27) Kondo, T.; Kato, H. S.; Bonn, M.; Kawai, M. Morphological change during crystallization of thin amorphous solid water films on Ru (0001). *J. Chem. Phys.* **2007**, *126*, 181103.

(28) Jardine, A.; Hedgeland, H.; Alexandrowicz, G.; Allison, W.; Ellis, J. Helium-3 spin-echo: Principles and application to dynamics at surfaces. *Prog. Surf. Sci.* **2009**, *84*, 323–379.

(29) Alexandrowicz, G.; Jardine, A. Helium spin-echo spectroscopy: studying surface dynamics with ultra-high-energy resolution. *J. Phys. Condens. Matter* **2007**, *19*, 305001.

(30) Farias, D.; Rieder, K.-H. Atomic beam diffraction from solid surfaces. *Rep. Prog. Phys.* **1998**, *61*, 1575.

(31) Batsanov, S. Van der Waals radii of elements. *Inorg. Mater.* **2001**, *37*, 871–885.

(32) Zeppenfeld, P.; Kern, K.; David, R.; Comsa, G. Diffraction from domain-wall systems. *Phys. Rev. B* **1988**, *38*, 3918.

(33) Kern, K.; Zeppenfeld, P.; David, R.; Comsa, G. Two-dimensional phase transitions studied by thermal He scattering. *J. Vac. Sci. Technol., A* **1988**, *6*, 639–645.

(34) Redhead, P. Thermal desorption of gases. *Vacuum* **1962**, *12*, 203–211.

(35) King, D. A. Thermal desorption from metal surfaces: A review. *Surf. Sci.* **1975**, *47*, 384–402.

(36) Günther, S.; Menteş, T.; Niño, M.; Locatelli, A.; Böcklein, S.; Wintterlin, J. Desorption kinetics from a surface derived from direct imaging of the adsorbate layer. *Nat. comm.* **2014**, *5*, 4853.

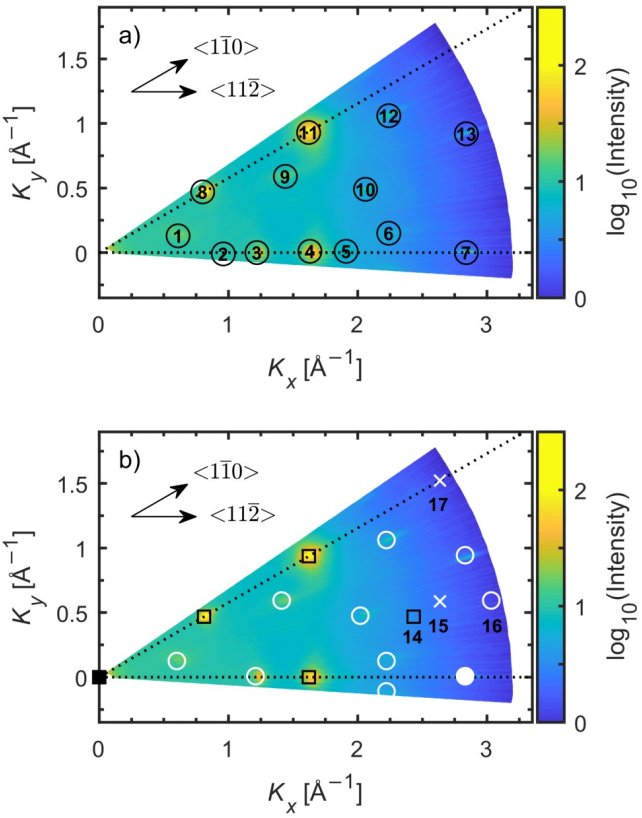

Figure 1: (a) 2D diffraction pattern of a COT adlayer at 205 K after dosing to saturation at 230 K. K_x and K_y are the x- and y-components of the surface-parallel momentum transfer. All observed peaks are labeled with numbers. Dotted lines and arrows represent the high symmetry directions of the Cu(111) surface and are determined by the position of the Cu(111) first-order diffraction peak 7. (b) Experimental diffraction pattern overlayed with the expected pattern. The white circles result from a convolution of the reciprocal lattice of COT (black squares) with the first-order Cu(111) peaks (filled white circle). White crosses denote the convolution with higher-order Cu(111) peaks. Only the first four sets of COT diffraction peaks have been used for the convolution.

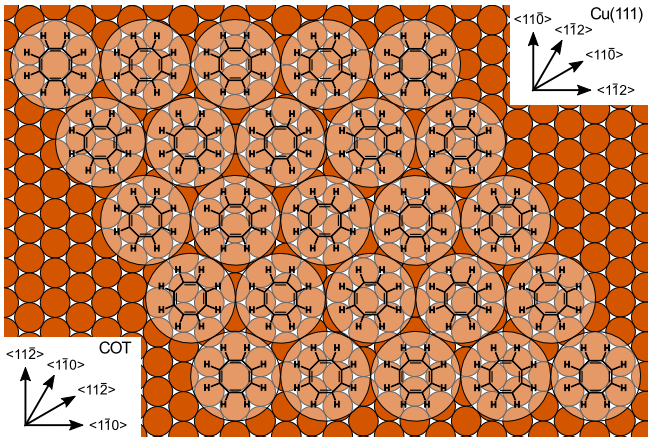

Figure 2: Schematic representation of the hexagonal close-packed structure, $(3 \times 3)R30°$, of a COT monolayer on Cu(111). Cu atoms are drawn by filled circles. The circles drawn around the COT molecules indicate the van der Waals radius of COT based on the estimated lattice constant of the monolayer structure. The inlets show the high symmetry directions of the Cu(111) surface and the COT adlayer. The orientation of the individual COT molecules with respect to the surface is shown for illustration only.

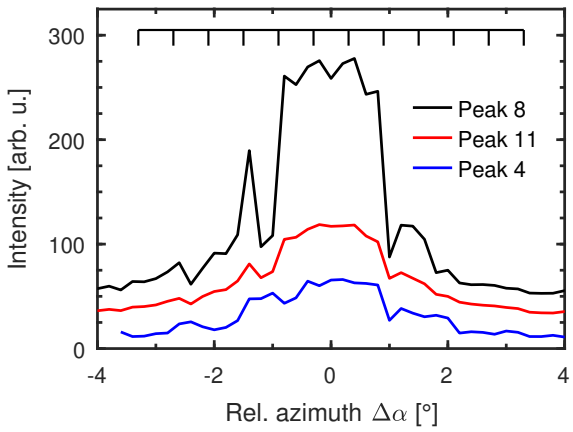

Figure 3: Azimuthal fine structure of the main COT diffraction peaks (1,0), (2,0) and (1,1) at 205 K (peaks 8, 11 and 4 in Fig1(a)), which are given as black, red and blue lines, respectively. The azimuthal angles $\Delta\alpha$ are given relative to the corresponding peak centers. A comb of angles evenly spaced by 0.6° and centered at $\Delta\alpha = 0°$ is shown above the peaks.

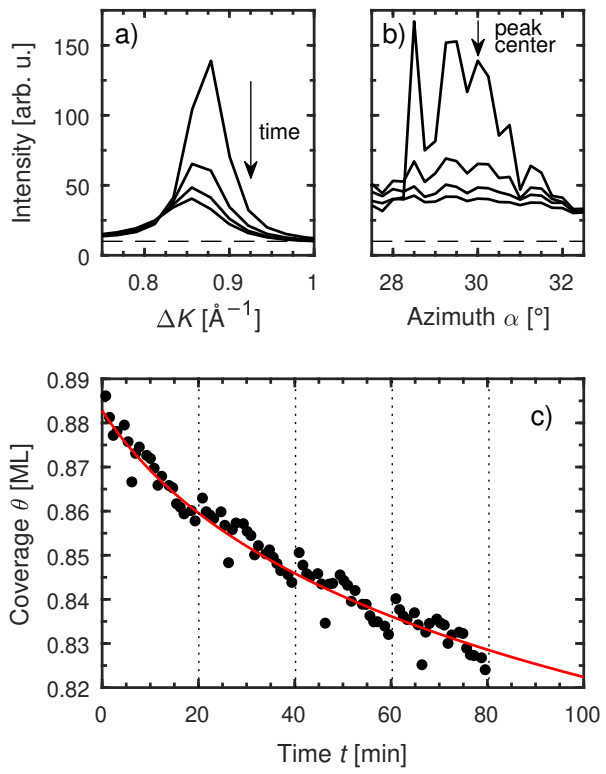

Figure 4: Temporal evolution of peak 8 during isothermal desorption after dosing to saturation at 300 K. Shown are four consecutive 2D diffraction scans (20 min per scan). Each 2D scan is composed of 21 angular scans measured for azimuthal angles between 27.5 and 32.5 degrees. a) Evolution of angular scans at the peak center ($\alpha = 30^{\circ}$). b) Azimuthal dependence of the peak maxima in a). The asymmetric shape of the peaks arises because desorption occurs while measuring the 2D scans and α is scanned towards positive values. c) Temporal evolution of the coverage (relative to the monolayer coverage at 205 K), which is calculated from the ΔK values of the intensity maxima for each angular scan. The red line corresponds to the fit described in the text and dotted lines indicate the end of each 2D scan.

Graphical TOC Entry